Biosensors and Bioelectronics 137 (2019) 110–116

Contents lists available at ScienceDirect

Biosensors and Bioelectronics

journal homepage: www.elsevier.com/locate/bios

Highly sensitive fluorescence biosensor for intracellular telomerase detection based on a single patchy gold/carbon nanosphere via the combination of nanoflare and hybridization chain reaction

Xiaoxiao Wang[a], Dandan Yang[a], Mei Liu[a], Dongwei Cao[b,*], Nongyue He[c,**], Zhifei Wang[a,***]

[a] Pharmaceutical Research Center, Jiangsu Province Hi-Tech Key Laboratory for Biomedical Research, School of Chemistry and Chemical Engineering, Southeast University, Nanjing, Jiangsu, 211189, China
[b] Department of Nephrology, Affiliated Drum Tower Hospital, Medical School of Nanjing University, Nanjing, 210008, China
[c] School of Biological Science and Medical Engineering, Southeast University, Nanjing, 210096, China

ARTICLE INFO

Keywords:
Intracellular telomerase
Biosensor
Signal amplification
Hybridization chain reaction
Nanoflare

ABSTRACT

How to *in situ* detect intracellular telomerase activity with high sensitivity still faces many challenges. This paper constructs a new fluorescence biosensing platform for the sensitive detection of intracellular telomerase activity via the combination of nanoflare and hybridization chain reaction (HCR)-based signal amplification on a single patchy gold/carbon nanosphere (PG/CNS), which has two or more distinct parts and allows hybridized-DNA (HS-DNA/Primer-DNA/Flare-DNA) and H1/H2-DNA (a pair of cross complementary DNA hairpins) to bind onto their surfaces via Au–S bond and electrostatic interaction, respectively. In the presence of telomerase, Primer-DNA (telomerase primer) extends at its 3′ end to produce a telomeric repeated sequence, resulting in the release of Flare-DNA followed by the recovery of the fluorescence. Subsequently, the released Flare-DNA further initiates cross hybridization of H1 and H2 DNA from mimic-HCR system to amplify the fluorescence signal. The in vivo confocal microscopy studies demonstrate that resulting sensor can enter into the cancer cells such as A549 cells, and lead to the increase in luminescence, which is stronger than the sensor without the HCR-based signal amplification system. A linear relationship between the fluorescence intensity and the amount of A549 cells is observed, and the limit of detection of the sensor reaches about 280 A549 cells.

1. Introduction

Telomerase, also called terminal transferase, plays an important role in preserving the telomeric length via catalyzing the addition of hexametric TTAGGG repeats onto the 3′-ends of chromosomes (Yorin, 1989; Blasco, 2005; Tian and Weizmann, 2013; Zhou et al., 2009). Telomerase expression is found to be elevated in over 85% of all known human malignant cells but be repressed in normal cells (Hahn et al., 1999; Hanahan and Weinberg, 2000; Masutomi et al., 2003). Therefore, telomerase expression level has been considered to be closely correlated to the occurrence of tumor, and the corresponding detection in clinic is thus of special importance for the early cancer diagnosis (Xiong et al., 2017). To date, polymerase chain reaction (PCR)-based telomere repeat amplification protocol (TRAP) (Xiao et al., 2010; Herbert et al., 2006) and PCR-free methods, such as electrochemistry (Pavlova et al., 2004; Ling et al., 2016; Mori et al., 2013), electrochemiluminescence (Xiong et al., 2017; Zhang et al., 2014; Wang et al., 2015), and fluorescence resonance energy transfer (FRET) based fluorescence approaches (Zhuang et al., 2015; Wang et al., 2016a,b; Ning et al., 2017; Ou et al., 2017), have been separately developed to assay telomerase. However, in spite of the above advances, most of biosensing platforms just meet the requirement to determine the activity of telomerase from tumor cell lysates and fail to provide *in situ* telomerase information in individual cell. Therefore, how to construct an effective biosensing platform to *in situ* detect intracellular telomerase activity with high sensitivity is highly desired and remains a challenge.

Meanwhile, with the great achievement in synthesis of nanomaterials in past decades, various functional nanomaterials have been widely employed in the fabrication of biosensor. In order to detect the telomerase of living cells, it is a common agreement that the sensor should not only have the high efficiency in entering live cells but also possess smart response system which only yields the signal quantitatively in the

* Corresponding author.
** Corresponding author.
*** Corresponding author.
E-mail addresses: cdwlqq@hotmail.com (D. Cao), nyhe@seu.edu.cn (N. He), zfwang@seu.edu.cn (Z. Wang).

https://doi.org/10.1016/j.bios.2019.05.004
Received 23 January 2019; Received in revised form 13 April 2019; Accepted 2 May 2019
Available online 06 May 2019
0956-5663/

presence of telomerase. Therefore, the biosensor prepared by the combination of “turn off-on” fluorescence probe and functional nanoparticle in a single construct has been focusing many attentions on account of the big improvement on the cellular uptake efficiency brought by nanoparticles. For example, in 2013, Ju's (Qian et al., 2013) group first reported the fabrication of telomerase-responsive mesoporous silica nanoprobe, which releases the embedded fluorescein in the presence of telomerase. In 2014, to overcome the complicated fabrication procedure and a certain degree of nonspecific release involved in above approach, they designed another Nicked molecular beacon-functionalized sensor by using Au NPs as fluorescence quenchers (Qian et al., 2014). In spite of the above improvement, as Tang's (Hong et al., 2016) group pointed out, its sensitivity is limited due to the one-to-one response of fluorescence signal to telomerase. Therefore, to further enhance the sensitivity, the signal amplification-based strategy should be employed in the design of biosensor for *in situ* monitoring of telomerase activity.

As an amplifying signal transducer, hybridization chain reaction (HCR) does not require the participation of the enzyme and can utilize a cascade of hybridization events by means of a pair of cross complementary DNA hairpins (H1-DNA and H2-DNA) to amplify the signal (Wu et al., 2015a; Chen et al., 2012; Hou et al., 2015; Zheng et al., 2014; Lu et al., 2017; Yang et al., 2012), thus becoming a powerful tool in the detection of mRNA (Wu et al., 2015b) in live cells and of protein (Zhang et al., 2012). In 2016, Tang's (Hong et al., 2016) group reported an enzyme-free signal amplification-based assay for telomerase by jointly using gold nanoflare and graphene oxide-loaded HCR system, where the delivery of trigger-DNA and H1/H2-DNA into the cell is conducted by gold nanoparticle and graphene oxide, separately. However, the different cell uptake efficiency of gold nanoflare and graphene oxide will greatly affect their cooperation on the amplification of signal, thus decreasing the detection sensitivity. As an emerging class of nanomaterials, Janus or patchy nanoparticle (Hu et al., 2012; Gro¨schel et al., 2012; Bradley et al., 2016. Loget et al., 2012) with the surface divided into two or more distinct parts can allow two different types of surface chemical modification to occur on the same particle, which opens the opportunity in the design and corresponding fabrication of new sensor. Spurred by our previous work (Wang et al., 2016b) on the synthesis of patchy gold on carbon nanospheres (PG/CNSs), herein, we propose a single PG/CNS-based biosensor for intracellular telomerase detection via the combination of nanoflare and hybridization chain reaction.

We first synthesized carbon nanospheres (CNSs) using the facile hydrothermal carbonization of glucose and then covered their surfaces with thin gold patch via the adsorption-reduction method. With the assistance of strong Au–S bonds, “hybridized-DNA” (HS-DNA/Primer-DNA/Flare-DNA, the corresponding sequence can be found in Supporting information Table S1) can selectively bind to the surface of patchy gold to form the sensor 1, which is similar to the fabrication of.

Conventional nanoflare (Prigodich et al. 2009, 2012). Under this condition, the fluorescence of FAM from Flare-DNA terminal is quenched due to the FRET between dye and Au. In the presence of the telomerase, which can elongate the telomere-primer (Primer-DNA), Flare-DNA will be replaced and further dissociate from “hybridized-DNA” with the simultaneous recovery of the fluorescence (Step 1). To fabricate HCR-based signal amplification system, two FAM-labeled hairpin-structured DNA probes H1-DNA/H2-DNA (the corresponding sequence can be found in Table S1) are further self-assembled onto the remains of carbon sphere's surface via the electrostatic interaction between the negative backbone of H1-DNA/H2-DNA and the positive amine group of branched polyethylenimine (PEI) from carbon sphere's surface, and the resulting sensor is called PG/CNSs mimic-HCR sensor (also to be called sensor 2 later) (Scheme 1A). Similarly, no fluorescence signal is observed for sensor 2 due to the fluorescence quenching effect of CNSs on the adsorbed H1/H2-FAM. After the sensor 2 is endocytosed into cells (Scheme 1B), if there is some intracellular telomerase, the released

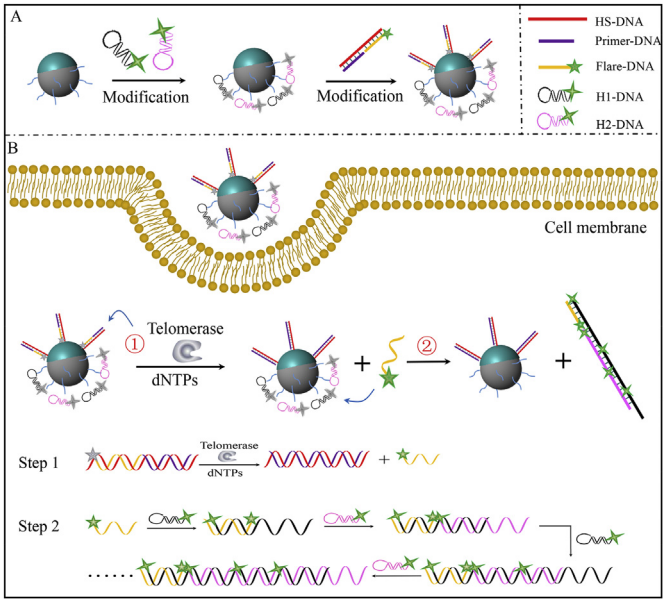

Scheme 1. (A) Schematic diagram of the preparation process of PG/CNS-based sensor. (B) Schematic illustration of PG/CNSs-based mimic-HCR sensor for *in situ* detection of intracellular telomerase.

Flare-DNA can work as the initiator to trigger a cascade of the alternative hybridization of H1-DNA and H2-DNA to form the nicked double helices (Step 2). Afterwards, the HCR product will detach from the surface PG/CNSs, leading to the recovery of the fluorescence and thus the amplification of the detection signal. In comparison with one-to-one response of fluorescence signal (Qian et al., 2014; Wang et al., 2016a; Ou et al., 2017), herein, the introduction of HCR is expected to improve the sensitivity. Therefore, the PG/CNSs-based mimic-HCR biosensing platform provides a convenient and sensitive method for telomerase detection, especially for *in situ* fluorescence imaging.

2. Experimental section

2.1. Materials

All chemicals and apparatus involved in the experiment have been given in supporting information and used as received.

2.2. Synthesis of PG/CNSs

The detail procedure for the synthesis of PG/CNSs had been shown in our previous work (Wang et al., 2016a,b), and resulting PG/CNSs was eventually dispersed in water with a concentration of 1 mg mL^{-1}.

2.3. Preparation of hybridized DNA-modified PG/CNSs sensor (sensor 1) and H1/H2-PG/CNSs mimic-HCR sensor (sensor 2)

Sensor 1: First, Flare-DNA (100 μL, 10 μM), Primer-DNA (100 μL, 10 μM), and HS-DNA (100 μL, 10 μM) were mixed and heated up to 75 °C. After 20 min, the mixture was slowly cooled in the dark to facilitate DNA hybridization. Considering the fact that the residual amino groups (from PEI group) on the surface of the PG/CNSs would non-specifically adsorb hybridized-DNA, we further blocked the amino group with mPEG-COOH (MW = 5 kDa), which was activated for 0.5 h by utilizing EDC and NHS, prior to the modification of hybridized-DNA. After that, the obtained PG/CNSs (0.1 mL, 1 mg/mL) and hybridized-DNA (20 μL) was mixed and incubated at 4 °C for at least 12 h. Next, the mixture was centrifuged and washed with PBS. Finally, sensor 1 was re-dispersed in 0.1 mL of PBS buffer for reserve.

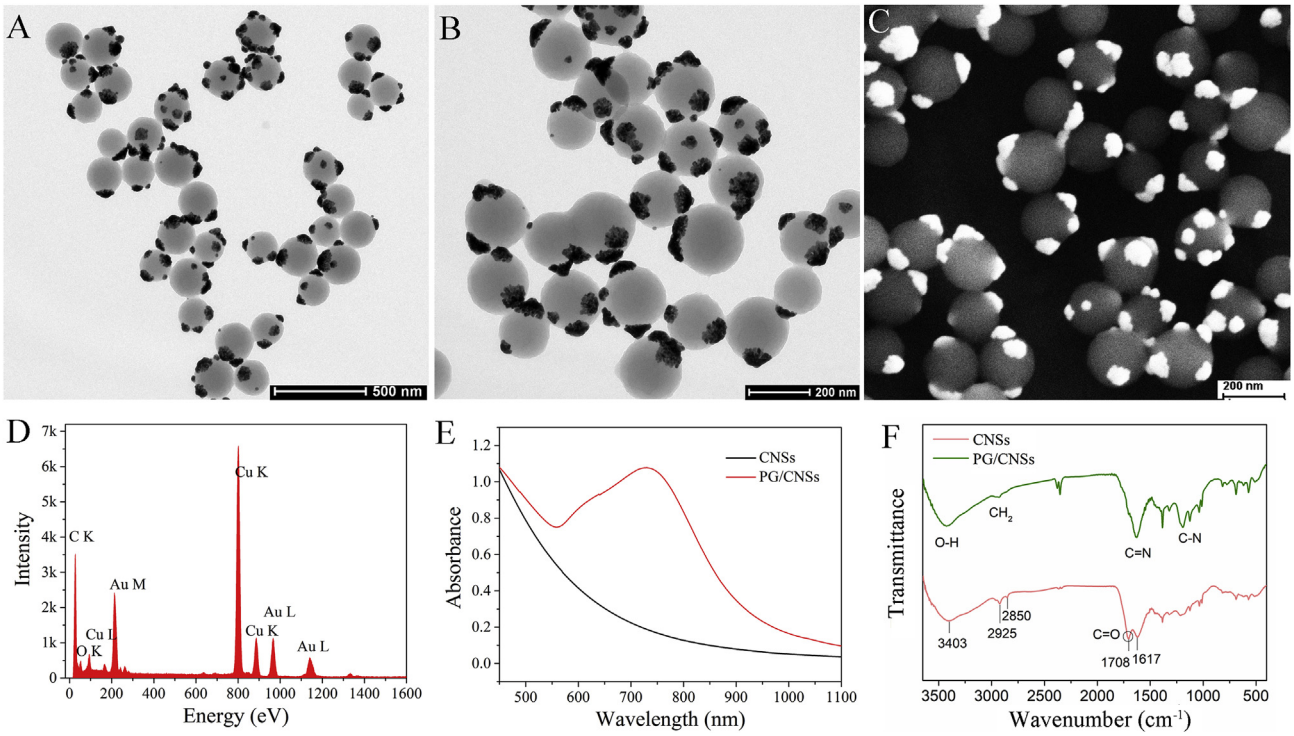

Fig. 1. TEM (A, B) and SEM (C) images of PG/CNSs; EDX pattern of PG/CNSs (D); UV–vis–NIR absorbance spectra (E) and FT-IR spectra (F) of CNSs and PG/CNSs.

Sensor 2: First, H1-DNA and H2-DNA were respectively heated at 75 °C for 20 min, and then cooled naturally to form a hairpin structure. After that, to optimize the concentration of PG/CNSs, different amounts of PG/CNSs (0, 10, 25, 50, 75, 100, 125, 150 and 175 μg/mL) were mixed with the mixture of H1-DNA and H2-DNA (The final concentration of both H1-DNA and H2-DNA were 70 nM), and the corresponding fluorescence intensity was detected at the excitation of 488 nm. In the subsequent experiment, the optimized concentration of PG/CNSs was 75 μg/mL (See Fig. S1 in Supporting Information). After electrostatic adsorption for 1 h,hybridized-DNA was added into the above solution, followed by the incubation at 4 °C for at least 12 h. Next, the resulting PG/CNSs were centrifuged, washed and incubated with the mixture of H1 and H2 (70 nM) again. Finally, sensor 2 was obtained by separating PG/CNSs from the mixture solution with the centrifugation.

2.4. Preparation of telomerase extracts

The human lung cancer cells (A549 cells) in the exponential growth phase were collected, and 1×10^6 cells suspension was added into a centrifuge tube, then washed three times with PBS and resuspended in 200 μL of CHAPS lysis buffer. After incubation for 30 min on ice, the supernatant was collected by centrifugation at 4 °C for use.

2.5. Telomerase response experiment

To investigate the response of sensor 1 to telomerase, 20 μL of dNTPs (10 mM) and 10 μL of telomerase extracts were introduced into sensor 1 (70 μL, 75 μg/mL). After incubation for different time, the fluorescence of corresponding solution between 500 and 650 nm was detected at the excitation of 488 nm. As a control, only dNTPs without telomerase was introduced into another solution containing sensor 1 too.

2.6. Fluorescence recovery of H1/H2-PG/CNSs mimic-HCR system

Different concentrations of Trigger-DNA (0, 10 15, 20, 25, 35, 80, 120, 200 nM) was incubated with sensor 2 (100 μL, 75 μg/mL) for 4 h. And then the fluorescence intensity of solution was measured by fluorescence spectrometer.

2.7. Detection of telomerase activity in cell extracts

To 10 μL of A549 cells extract (the number of cells: 0, 1000, 2000, 4000, 5000, 7500, 10000, 15000, 20000), dNTPs (10 μL, 10 mM), and sensor 1/or sensor 2 (300 μL) were added. And the resulting solutions were incubated at 37 °C. After 2 h, the corresponding fluorescence between 500 and 650 nm was measured by a Fluorescence Spectrometer (λ_{ex} = 488 nm).

2.8. Detection of telomerase activity in cell by using fluorescence imaging

After A549 cells were seeded in a confocal dish and incubated for 24 h, the medium was removed, and then sensor 1, sensor 2 or pure mimic-HCR system (without hybridized-DNA) was added and further incubated with cells for another 6 h, respectively. The fluorescence microscopic images of cells were taken using a laser scanning confocal microscope. Similarly, MCF-7, HepG2 or L929 cells were further detected instead of A549 cells.

For the verification of the sensor's specificity, A549 cells in cell-adhered dish were incubated with 60, 120, or 240 μg mL^{-1} epigallocatechin gallate (EGCG, a telomerase-inhibiting drug) for 24 h in advance. After that, sensor 2 was added and incubated with cells for another 6 h. Finally, the cells were observed under fluorescent confocal microscope.

3. Results and discussion

3.1. Synthesis and characterization of sensor 1 and sensor 2

As an important part of proposed biosensor, PG/CNSs were synthesized by the facile adsorption-reduction method (Wang et al., 2016a,b). To understand the morphology of the resulting PG/CNSs nanocomposite, we performed TEM and SEM characterization. As

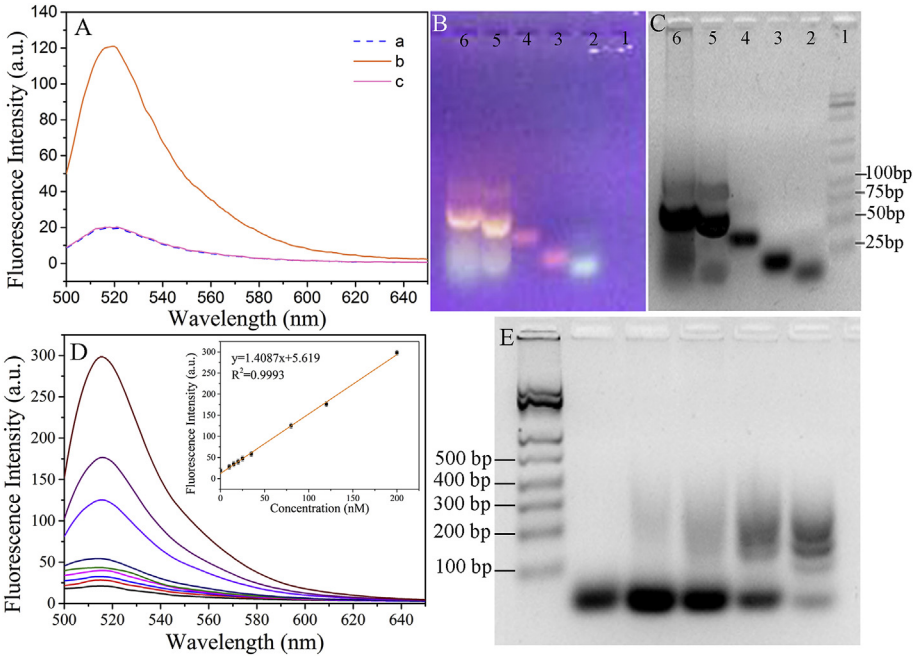

Fig. 2. (A) Fluorescence spectra of the sensor 1 (curve a), sensor 1 and dNTPs in the presence (curve b) or absence (curve c) of telomerase; (B, C) Analysis of gel electrophoresis for telomerase-triggered Primer-DNA extension and Flare-DNA release. (1: maker DNA, 2: Flare-DNA; 3: Primer-DNA; 4: HS-DNA; 5: hybridized-DNA + dNTPs; 6: hybridized-DNA + dNTPs + telomerase); (D) Fluorescence recovery after adding Trigger DNA (0, 10 15, 20, 25, 35, 80, 120, 200 nM) into PG/CNSs mimic-HCR system (75 μg mL^{-1}), Insert: the plot of fluorescence intensity recorded at 515 nm *vs.* the concentration of Trigger DNA. (E) Analysis of gel electrophoresis for Flare-DNA initiated mimic-HCR. (1: maker DNA, 2: H1-DNA, 3: H1-DNA + H2-DNA, 4: H1-DNA + H2-DNA + 0.25 μM Flare-DNA, 5: H1-DNA + H2-DNA + 1 μM Flare-DNA, 6: H1-DNA + H2-DNA + 2.5 μM Flare-DNA after incubation for 2 h).

shown in Fig. 1A and B, we can see that obtained PG/CNSs own the uniform morphology with almost each surface covered by several gold patches (the dark part) with the size of 60 nm. The average diameter of whole particle is approximately 180 nm, and gold patches just occupy the small area of the carbon nanosphere, which thus allows two different types of surface chemical modification to occur on the same particle. Such characteristic structure is also verified by SEM image (Fig. 1C), in which the bright gold patches resulting from the high conductivity of Au and the dark carbon surface is spatially well-separated. In order to analyze the chemical composition of PG/CNSs, Fig. 1D gives the corresponding EDX spectrum, and it can be seen that in addition to the Cu substrate, both Au and C species are present. The UV–vis–NIR absorption of PG/CNSs is also given in Fig. 1E, and we can find that there is the broad absorption between 600 nm and 850 nm resulting from the formation of patch gold. Fig. 1F illustrates the FT-IR spectrum of the resulting PG/CNSs. In.

Comparison with the spectrum of CNSs, it can be found that the characteristic peak of C = O group (1708 cm^{-1}) in CNSs disappears and two new peaks appear. The absorption peak at about 1000–1200 cm^{-1} can be attributed to C–N stretching vibration of PEI, and the absorption peak at 1617 cm^{-1} is caused by stretching vibration of C = N groups formed by the reaction between CHO groups of CNS and NH_2 groups of PEI. These evidences indicate the presence of PEI on the surface of PG/CNSs. Therefore, it is expected that resulting PG/CNSs can be used for the subsequent self-assembly of "hybridized-DNA" and H1/H2-DNA.

To better understand the PG/CNSs-based mimic-HCR strategy, the sensor 1 is first fabricated by only binding "hybridized-DNA" to the surface of patchy gold with the assistance of strong Au–S bonds. To avoid the nonspecial adsorption of "hybridized-DNA" on other parts of carbon nanosphere, the surface of PG/CNSs was further blocked by mPEG-COOH modification through the reaction between amine group of PEI and carboxyl group of mPEG-COOH before they are used for the self-assembly of sensor 1. In comparison with PG/CNSs, the average hydrodynamic size of mPEG-modified PG/CNSs increases from 180 nm to 215 nm (Fig. S2A, curve a, b), and the corresponding zeta potential obviously decreases from +22.5 mV to +3.9 mV (Fig. S2B, a and b), indicating that mPEG-COOH has been successfully grafted on the PG/CNSs' surface. "Hybridized-DNA" was bound to the surface of patchy gold from PG/CNSs by incubating the mixture solution of "hybridized-DNA" and mPEG-modified PG/CNSs at 4 °C for 12 h. According to the mercaptoethanol competing experiment, the amount of the hybridized-DNA assembled on each PG/CNS is about 4480 (Fig. S3 gives the process of determination) under the optimized experiment condition. After the attachment of "hybridized-DNA", the average hydrodynamic size of resulting sensor 1 further increases to 226 nm (Figs. S2A and c), and the corresponding zeta potential decreases to −8.4 mV (Figs. S2B and c).

In comparison with sensor 1, sensor 2 was fabricated by additionally adsorbing H1/H2-DNA on residual parts of carbon nanosphere. In the experiment, PG/CNSs without PEGylation were first incubated with H1/H2-DNA. After the adsorption, the fluorescence intensity of the supernatant was significantly reduced, indicating that H1/H2-DNA was successfully adsorbed on the surface of PG/CNSs via electrostatic interaction (Fig. S4C). According to the decrease in fluorescence intensity, we deduce that the total amount of the H1/H2-DNA adsorbed on each PG/CNS is about 14170 after optimizing the experiment condition (Fig. S5 gives the process of determination). A similar synthetic procedure to sensor 1 was next performed to attach "hybridized-DNA" to H1/H2-DNA modified PG/CNSs. After the formation of sensor 2, the final hydrodynamic size of resulting PG/CNS is about 208 nm (Fig. S4A, curve c), and the zeta potential changes to −12.4 mV (Figs. S4B and c).

3.2. *In vitro* studies of telomerase activity with sensors

Before the evaluation of sensor 2, we first *in vitro* studied the response of "hybridized-DNA", which consists of HS-DNA/Primer-DNA/Flare-DNA, to Telomerase with sensor 1. As mentioned above, the fluorescence of Flare-DNA in sensor 1 is nearly quenched by Au due to the FRET mechanism. Therefore, only a very small amount of fluorescence was detected in the aqueous solution containing sensor 1, as shown in Fig. 2A (curve a). With the addition of telomerase and dNTP into above solution, the fluorescence intensity is significantly enhanced after 2 h incubation, which suggests that Flare-DNA has dissociated from sensor 1 successfully (curve b). In the control group, no obvious increase in fluorescence intensity is observed when only dNTP is added (curve c), further demonstrating that the release of Flare-DNA is induced by the telomere-primer extension under the catalysis of Telomerase. To optimize the reaction condition, we also investigated the effect of incubation time on the corresponding fluorescence intensity. As shown in.

Fig. S6, with the increase in incubation time, the fluorescence

intensity gradually increases and reaches the maximum in 70 min (line b) after the addition of telomerase and dNTP. Meanwhile, it can be also found that in the absence of telomerase, the fluorescence intensity has no obvious change in the control group in 2 h (line a), demonstrating the good stability of sensor 1.

In addition, agarose gel electrophoresis was also performed to verify the telomerase-triggered Primer-DNA extension and Flare-DNA release. As shown in Fig. 2B, in comparison with single strand HS-DNA (lane 4), "hybridized-DNA" (lane 5) has larger size and exhibits strong fluorescence due to the formation of double strand with Flare-DNA (lane 2) and Primer-DNA (lane 3). However, "hybridized-DNA" incubated with both dNTPs and telomerase (lane 6) shows more trailing than "hybridized-DNA", and the size of DNA piece which exhibits the fluorescence is similar to that of Flare-DNA, verifying the release of Flare-DNA resulting from telomerase-triggered Primer-DNA extension.

We next investigated whether the released Flare-DNA could trigger a cascade of the alternative hybridization of H1-DNA and H2-DNA to form the nicked double helices, further resulting in the signal amplification, or not. To avoid the interference of FAM from Flare-DNA on the fluorescence intensity resulting from the hybridization of H1/H2-DNA, Trigger-DNA (with the same DNA sequence to Flare-DNA) was used. With the introduction of increasing amount of the Trigger-DNA, the intensity of the fluorescence linearly increases (Fig. 2D), indicating that the mimic-HCR system can be used for the signal amplification. Moreover, the Trigger-DNA induced-hybridization of H1/H2-DNA was verified by gel electrophoresis. As shown in Fig. 2E, it can be seen that most of H1/H2-DNA exist in the form of monomers before the addition of Trigger-DNA. However, as the concentration of Trigger-DNA increases, the trailing phenomenon of the gel becomes more and more obvious and the luminance of the monomers is getting weaker and weaker (from lines 4, 5, and 6), which indicates that the amount of longer double helix structure is increasing and the corresponding monomers is decreasing simultaneously. Therefore, it is concluded that released Flare-DNA can be used for the initiation of the mimic-HCR.

3.3. *In situ fluorescence imaging of intracellular telomerase activity*

Before being used for the detection of telomerase activity in cells, the cytotoxicity of sensor 2 was determined by MTT assay with MCF-7 cells. Fig. S7 gives the MCF-7 cell viability after 24 h incubation with various concentrations of sensor 2. It can be found that more than 95% of MCF-7 cells are still alive even at high concentration of 1000 μg/mL, indicating that the cytotoxicity of sensor 2 is negligible and it is suitable for further detection of intracellular telomerase.

A549 cells with high telomerase activity were employed to *in situ* evaluate the performance of sensor 2, and both sensor 1 and PG/CNSs mimic-HCR sensor without the attachment of hybridized-DNA were used as the control group, respectively. In the experiment, A549 cells were first incubated with these sensors for 6 h, and then washed with PBS to remove free nanoparticles. As shown in Fig. 3A, as for sensor 2, a strong fluorescence is observed inside A549 cells when.

Compared with sensor 1, in which there is the relatively weak fluorescence inside cells. However, in the case of A549 cells treated with PG/CNSs mimic-HCR sensor without the attachment of hybridized-DNA, almost no fluorescent signal is observed, indicating that only mimic-HCR system can't lead to the fluorescence recovery. These results comparatively demonstrate that the generation of fluorescence inside cells treated with sensor 1 or sensor 2 is really induced by their telomerase which leads to the release of Flare-DNA accompanied by the opening of fluorescence signal (sensor 1) and the subsequent hybridization of H1/H2-DNA in the mimic-HCR system (sensor 2). As mentioned in the introduction, as for sensor 1, the fluorescence just comes from the released Flare-DNA. However, the fluorescence as to sensor 2 is further amplified by the subsequent hybridization of H1 and H2-DNA. That is why the fluorescence inside cells treated with sensor 2 appears stronger than that inside cells treated with sensor 1. To verify the feasibility of the designed sensor for the detection of intracellular telomerase, sensor 2 was also used to evaluate the telomerase activity in another two different cancer cell lines HepG2 hepatocellular carcinoma and MCF-7 breast cancer. As shown in Fig. 3 B and C, similar to that of A549 cells, the fluorescence signal inside two different kinds of cells after 6 h incubation with sensor 2 can be observed and is also stronger than that inside cells treat with sensor 1. As we know, cancer cells always have high level of telomerase activity. Therefore, the results from A549 cells, HepG2 hepatocellular carcinoma and MCF-7 breast cancer, clearly demonstrate that obtained sensor 2 can enter into the cells, release the Flare-DNA under the catalysis of telomerase, and further amplify the signal via the HCR system.

As the control, sensor 2 was also incubated with normal cells L929 mouse fibroblasts cells and MCF-10A human mammary epithelial cells, where telomerase is absent, respectively. As shown in Fig. S8, there is no fluorescence signal under the confocal microscopy observation, further verifying that the generation of fluorescence in cancer cells incubated with sensor 2 can be attributed to the catalysis of telomerase. Thus, the constructed sensor 2 possesses the ability of sensitively detecting intracellular telomerase activity and of distinguishing cancer cells from normal cells.

3.4. *Sensitivity of DNA on PG/CNSs to nuclease degradation*

As we know, discrete DNA fragment can usually be degraded by intracellular nuclease. To investigate the stability of sensor 2 in physiological environment, DNase I was added into PBS solution containing sensor 2 to mimic this procedure. As shown in Fig. S9, there is the negligible fluorescence recovery whether in the presence of sensor 2/DNase I (line b) or sensor 2 alone in PBS (line a), indicating that no fragments from Flare-DNA or H1/H2-DNA is released into the solution and the oligonucleotides on the surface of PG/CNSs are highly resistant to DNase I. In this work, hybridized-DNA and H1/H2-DNA are tethered onto PG/CNSs via Au–S bond and electrostatic interaction, respectively. And such high DNA density and shorter oligonucleotides might increase protection of DNA against DNase I degradation. So, it is expected that obtained sensor 2 has the good stability after entering the cell, which provides the basis for its application in intracellular detection.

3.5. *Investigation of the inhibitory effect of EGCG on intracellular telomerase*

To confirm the specificity of our sensor to intracellular telomerase activity, sensor 2 was further employed for *in situ* evaluating the change of intracellular telomerase activity in response to telomerase inhibitor EGCG. In the experiment, A549 cells were pretreated with different concentrations of EGCG, and then incubated with sensor 2 for 6 h. As shown in Fig. 4, the fluorescence intensity from cells obviously decreases with increasing the concentration of EGCG, demonstrating that sensor 2 has a good specificity to telomerase activity.

3.6. *Fluorescence detection of telomerase activity in cell lysate with sensor 1 and sensor 2*

We also comparatively examined the sensitivity of the proposed PG/CNSs mimic-HCR sensor by detecting the telomerase activity in A549 cell extracts with sensor 1 and sensor 2, respectively. As shown in Fig. 5, the fluorescence signal increases linearly with the increasing of cell numbers from 0 to 20000 cells when the sensor was incubated with cell lysate and dNTPs for 2 h. For sensor 1 (Fig. 5A), the fluorescence signal only resulting from the dissociation of Flare-DNA on Au Patch is relatively weak and the limit of detection (LOD) is about 520 A549 cells. By contrast, sensor 2 (Fig. 5B) shows the strong fluorescence due to the integration between HCR-based signal amplification system and Flare-DNA, and the LOD reaches about 280 A549 cells. In addition, we also selected BSA, PDBF-BB, T4 ligase and heated telomerase as the

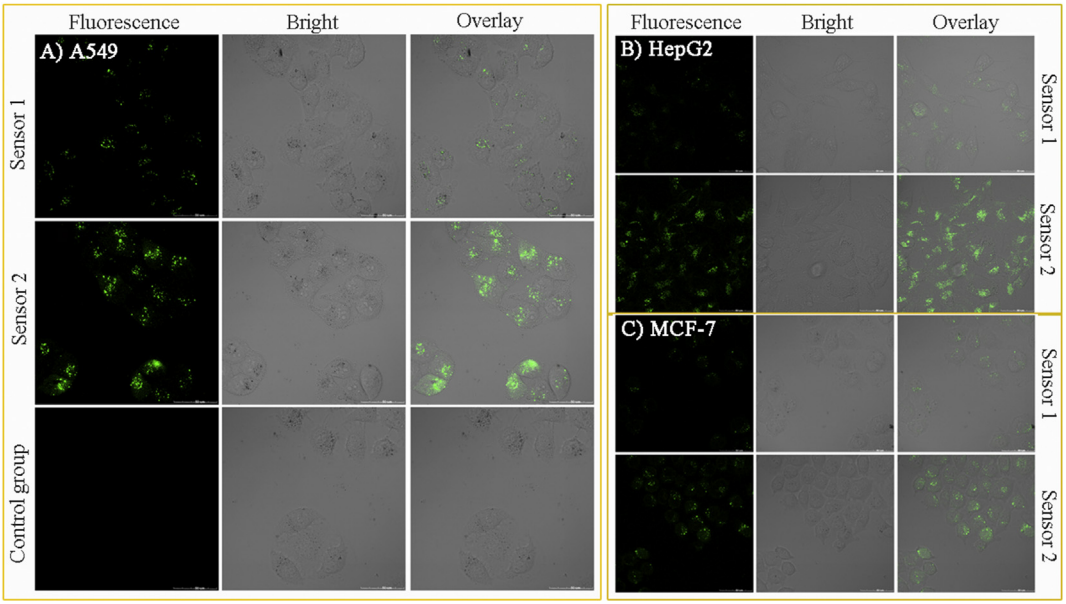

Fig. 3. (A) Confocal microscopic images of A549 cells after incubation with sensor 1, sensor 2, and PG/CNSs mimic-HCR sensor without the attachment of hybridized-DNA (control group); Confocal microscopic images of HepG2 (B) and MCF-7 (C) cells after incubation with sensor 1 and sensor 2.

possible interfering species based on the literature (Wang et al., 2019; Zhang et al., 2018) and further evaluated their interference on the detection of sensor 2. As shown in Fig. S10, no obvious increment in the fluorescence intensity was found in the control groups, where only interfering species were added. According to this result, we can find that the constructed sensor 2 has the good specificity for the detection of telomerase. So, it can be concluded that the HCR-based signal amplification has been well established in our work and the corresponding

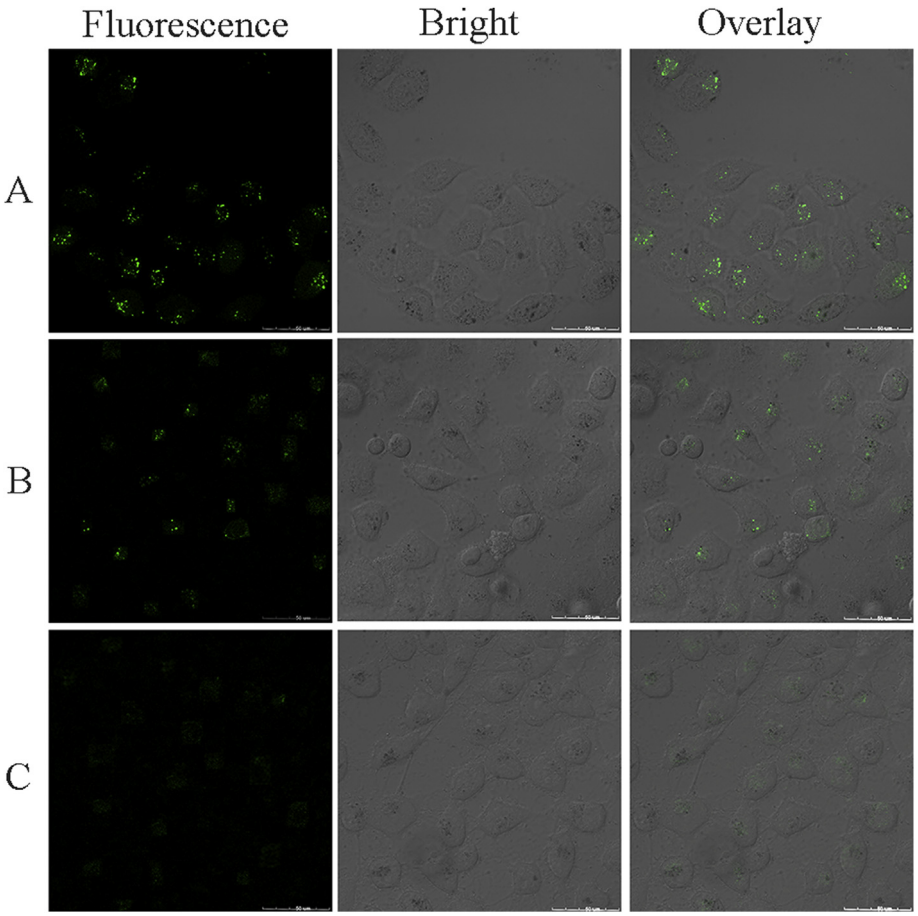

Fig. 4. Confocal microscopic images of A549 cells after the treatment with different concentration of EGCG ((A) 50, (B) 100, (C) 200 μg/mL) and subsequent incubation with sensor 2 for 6 h.

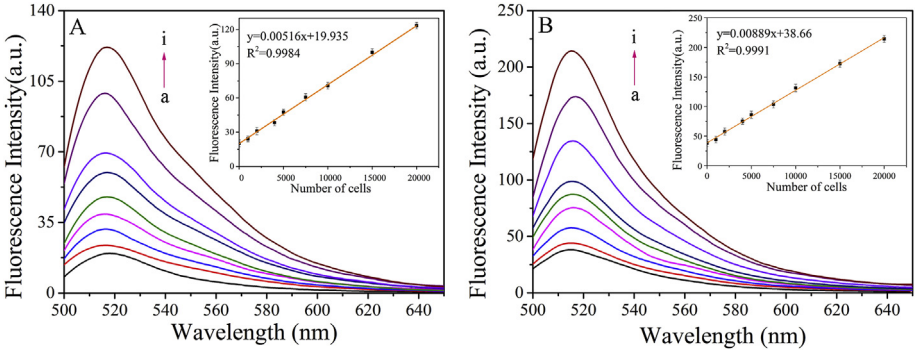

Fig. 5. Fluorescence spectra of the detection system by using sensor 1 (A) and sensor 2 (B). The different amounts of telomerase extracts from 0, 1000, 2000, 4000, 5000, 7500, 15000, 20000 A549 cells (a–i). Inset: The fluorescence intensity at 515 nm *vs.* the number of cells.

sensor 2 can be used for the detection of intracellular telomerase activity. When compared to other fluorescence assays for the detection of telomerase (Table S2), this work has a wide linear range, a short detection time, and especially can be used for *in situ* detection of telomerase in cell.

4. Conclusion

To conclude, in this work, an ultrasensitive fluorescence biosensor was developed to detect the intracellular telomerase activity by the combination of nanoflare and mimic HCR-based signal amplification system on a single PG/CNS with Janus structure. The in vivo confocal microscopy studies demonstrate that resulting sensor can enter into cancer cells, such as A549 cells, HepG2 cells, and MCF-7 cells, and lead to the increase in luminescence which is stronger than sensor without the HCR-based signal amplification system. By detecting the telomerase activity in A549 cell extracts, a linear relationship between the fluorescence intensity and the number of cells is observed, and the LOD of sensor reaches about 280 A549 cells. Considering the fact that PG/CNSs possess the good absorption in the range of 600 nm and 850 nm, it is also expected that resulting sensor can not only be employed for *in situ* monitoring the intracellular telomerase activity in cancer cells, but also be used as the photothermal agent for the photothermal treatment of cancer in future.

Conflict of interest

The authors declare no conflict of interest.

CRediT authorship contribution statement

Xiaoxiao Wang: Data curation, Formal analysis, Investigation, Software, Visualization, Writing - original draft. **Dandan Yang:** Formal analysis, Supervision, Validation, Visualization, Writing - original draft. **Mei Liu:** Supervision, Formal analysis. **Dongwei Cao:** Supervision, Writing - review & editing. **Nongyue He:** Supervision, Writing - review & editing, Funding acquisition, Project administration. **Zhifei Wang:** Resources, Methodology, Formal analysis, Supervision, Writing - review & editing, Funding acquisition, Project administration.

Acknowledgements

This study was financially supported by the NSF of China (81771976), Fundamental Research Funds for the Central Universities, the joint fund of Southeast University and Nanjing Medical University, and the Scientific Research Foundation of the Graduate School of Southeast University (YBJJ1789).

Appendix A. Supplementary data

Supplementary data to this article can be found online at https://doi.org/10.1016/j.bios.2019.05.004.

References

Gröschel, A.H., Walther, A., Löbling, T.I., Schmelz, J., Hanisch, A., Schmalz, H., Müller, A.H.E., 2012. J. Am. Chem. Soc. 134, 13850–13860.
Blasco, M.A., 2005. Nat. Rev. Genet. 6, 611–622.
Bradley, L.C., Stebe, K.J., Lee, D., 2016. J. Am. Chem. Soc. 138, 11437–11440.
Chen, Y., Xu, J., Su, J., Xiang, Y., Yuan, R., Chai, Y.Q., 2012. Anal. Chem. 84, 7750–7755.
Hahn, W.C., Stewart, S.A., Brooks, M.W., York, S.G., Eaton, E., Kurachi, A., Beijersbergen, R.L., Knoll, J.H.M., Meyerson, M., Weinberg, R.A., 1999. Nat. Med. 5, 1164–1170.
Hanahan, D., Weinberg, R.A., 2000. Cell 100, 57–70.
Herbert, B.-S., Hochreiter, A.E., Wright, W.E., Shay, J.W., 2006. Nat. Protoc. 1, 1583–1590.
Hong, M., Xu, L.D., Xue, Q.W., Li, L., Tang, B., 2016. Anal. Chem. 88, 12177–12182.
Hou, T., Li, W., Liu, X.J., Li, F., 2015. Anal. Chem. 87, 11368–11374.
Hu, J., Zhou, S.X., Sun, Y.Y., Fang, X.S., Wu, L.M., 2012. Chem. Soc. Rev. 41, 4356–4378.
Ling, P.H., Lei, J.P., Jia, L., Ju, H.X., 2016. Chem. Commun. 52, 1226–1229.
Loget, G., Roche, J., Kuhn, A., 2012. Adv. Mater. 24, 5111–5116.
Lu, S.S., Hu, T., Wang, S., Sun, J., Yang, X.R., 2017. ACS Appl. Mater. Interfaces 9, 167–175.
Masutomi, K., Yu, E.Y., Khurts, S., Benporath, I., Currier, J.L., Metz, G.B., Brooks, M.W., Kaneko, S., Murakami, S., DeCaprio, J.A., Weinberg, R.A., Stewart, S.A., Hahn, W.C., 2003. Cell 114, 241–253.
Mori, K., Sato, S., Kodama, M., Habu, M., Takahashi, O., Nishihara, T., Tominaga, K., Takenak, S., 2013. Clin. Chem. 59, 289–295.
Ning, D.H., He, C.T., Liu, Z.J., Liu, C., Wu, Q.L., Zhao, T.T., Liu, R.Y., 2017. Analyst 142, 1697–1702.
Ou, X.W., Hong, F., Zhang, Z.Y., Cheng, Y., Zhao, Z.J., Gao, P.C., Lou, X.D., Xia, F., Wang, S.T., 2017. Biosens. Bioelectron. 89, 417–421.
Pavlova, V., Willnera, I., Dishonb, A., Kotle, M., 2004. Biosens. Bioelectron. 20, 1011–1021.
Prigodich, A.E., Seferos, D.S., Massich, M.D., Giljohann, D.A., Lane, B.C., Mirkin, C.A., 2009. ACS Nano 3, 2147–2152.
Prigodich, A.E., Randeria, P.S., Briley, W.E., Kim, N.J., Daniel, W.L., Giljohann, D.A., Mirkin, C.A., 2012. Anal. Chem. 84, 2062–2066.
Qian, R.C., Ding, L., Ju, H.X., 2013. J. Am. Chem. Soc. 135, 13282–13285.
Qian, R.C., Ding, L., Yan, L.W., Lin, M.F., Ju, H.X., 2014. Anal. Chem. 86, 8642–8648.
Tian, L.L., Weizmann, Y., 2013. J. Am. Chem. Soc. 135, 1661–1664.
Wang, W.-J., Li, J.-J., Rui, K., Gai, P.-P., Zhang, J.-R., Zhu, J.-J., 2015. Anal. Chem. 87, 3019–3026.
Wang, Y.J., Yang, L.Z., Li, B.X., Jin, Y., 2016a. Analyst 141, 6133–6139.
Wang, X.X., Cao, D.W., Tang, X.J., Yang, J.J., Jiang, D.Y., Liu, M., He, N.Y., Wang, Z.F., 2016b. ACS Appl. Mater. Interfaces 8, 19321–19332.
Wang, J., Zhang, J., Li, T.T., Shen, R.D., Li, G.K., Ling, L.S., 2019. Biosens. Bioelectron. 131, 143–148.
Wu, Z., Liu, G.-Q., Yang, X.-L., Jiang, J.-H., 2015a. J. Am. Chem. Soc. 137, 6829–6836.
Wu, C.C., Cansiz, S., Zhang, L.Q., Teng, I.T., Qiu, L.P., Li, J., Liu, Y., Zhou, C.S., Hu, R., Zhang, T., Cui, C., Cui, L., Tan, W.H., 2015b. J. Am. Chem. Soc. 137, 4900–4903.
Xiao, Y., Dane, K.Y., Uzawa, T., Csordas, A., Qian, J.R., Soh, H.T., Daugherty, P.S., Lagally, E.T., Heeger, A.J., Plaxco, K.W., 2010. J. Am. Chem. Soc. 132, 15299–15307.
Xiong, C.Y., Liang, W.B., Zheng, Y.N., Zhuo, Y., Chai, Y.Q., Yuan, R., 2017. Anal. Chem. 89, 3222–3227.
Yang, L., Liu, C.H., Ren, W., Li, Z.Q., 2012. ACS Appl. Mater. Interfaces 4, 6450–6453.
Yorin, G.B., 1989. Cell 59 521-429.
Zhang, B., Liu, B.Q., Tang, D.P., Niessner, R., Chen, G.N., Knopp, D., 2012. Anal. Chem. 84, 5392–5399.
Zhang, H.-R., Wu, M.-S., Xu, J.-J., Chen, H.-Y., 2014. Anal. Chem. 86, 3834–3840.
Zhang, H., Lei, Z., Tian, R.R., Wang, Z.X., 2018. Talanta 178, 116–121.
Zheng, J., Hu, Y.P., Bai, J.H., Ma, C., Li, J.S., Li, Y.H., Shi, M.L., Tan, W.H., Yang, R.H., 2014. Anal. Chem. 86, 2205–2212.
Zhou, X.M., Xing, D., Zhu, D.B., Jia, L., 2009. Anal. Chem. 81, 255–261.
Zhuang, Y., Zhang, M.S., Chen, B., Duan, R.X., Min, X.H., Zhang, Z.Y., Zheng, F.X., Liang, H.G., Zhao, Z.J., Lou, X.D., Xia, F., 2015. Anal. Chem. 87, 9487–9493.